High-resolution study of ^{166}Er with the (p,t) reaction

D. Bucurescu,[1] S. Pascu,[1] G. Suliman,[1] H.-F. Wirth,[2] R. Hertenberger,[2] T. Faestermann,[3] R. Krücken,[4,5] and G. Graw[2]

[1]*Horia Hulubei National Institute of Physics and Nuclear Engineering, P.O. Box MG-6, R-76900 Bucharest, Romania*

[2]*Sektion Physik, Ludwig Maximilians Universität München, Am Coulombwall 1, 85748 Garching, Germany*

[3]*Physik Department, Technische Universität München, D-85748 Garching, Germany*

[4]*TRIUMF, British Columbia, Canada V6T 2A3*

[5]*Department of Physics & Astronomy, University of British Columbia, Vancouver, British Columbia, Canada V6T 1Z4*

(Received 26 March 2019; published 22 October 2019)

Excited states in the deformed nucleus ^{166}Er have been studied with high-energy resolution in the (p,t) reaction, with the Munich Q3D spectrograph. 143 states have been observed up to 4 MeV excitation, and spin and parity has been proposed for about 100 states, based on a DWBA analysis of their angular distributions, out of which 11 are excited 0^+ states, and 39 2^+ states. The excitation pattern of these states (especially the 0^+ ones) in ^{166}Er is compared to that in ^{168}Er. Calculations were carried out with the *spdf*-IBM model, which gives a reasonable agreement with the observed number of 0^+ states in ^{166}Er and their excitation in the (p,t) reaction. The $2n$-transfer intensity pattern for the 0^+ states in the ^{166}Er$(t,p)^{168}$Er reaction is also reasonably predicted. However, the *spdf*-IBM calculations do not explain the differences between ^{166}Er and ^{168}Er, in the (p,t) transfer distribution of the 0^+ states. The understanding of these differences, which appear to be related to a structure change at the $N = 98$ deformed subshell closure, remains as an important issue of future, more elaborated model calculations.

DOI: 10.1103/PhysRevC.100.044316

I. INTRODUCTION

The occurrence and evolution of different excitation modes in the rare-earth nuclei, which evolve from spherical to transitional and well-deformed nuclei, is of considerable interest. During recent years, a large number of excited states in these nuclei were revealed by high-energy resolution studies with the (p,t) direct reaction, which proved especially useful to unambiguously assign many 0^+ states [1–8]. As there are many various mechanisms that can form 0^+ states, the origin of these states was subject of many different approaches [4,9–15].

Up to about 3 MeV excitation, there is a wealth of information on the level scheme of the ^{166}Er nucleus, obtained from different experimental studies [16]. Low-spin states were studied with the β^- and EC decays [17–19], $(n,n'\gamma)$ reaction [20–22], inelastic scattering of protons [24] and of deuterons [25], Coulomb excitation [26], direct neutron transfer reactions [27–29], and (γ,γ') reaction [30], while higher spin states were studied with the $(\alpha,2n)$ reaction ([31] and references therein). Of relevance for the present study are the (t,p) and (p,t) reaction studies of this nucleus [32] and of ^{168}Er [4,33], and the (p,t) reaction studies of ^{160,162,164,166}Er [34,35], and of ^{164,166}Er [36].

^{166}Er is a deformed nucleus [$E(4^+)/E(2^+) = R(4/2) = 3.289$], with a low-energy level scheme very similar to that of its neighbor ^{168}Er [$R(4/2) = 3.309$]. Indeed, up to about 1.4 MeV the excitation energies of the ground and γ bands are almost identical, and the same is true for the first 3^- state and the 2γ 4^+ state at about 2.0 MeV [16]. Above an excitation energy of about 1.5 MeV the two nuclei show, nevertheless, differences in the energy distribution of the 0^+ and 2^+ states ([16] and present results). The two nuclei appear as rather different also in other properties of their excited 0^+ states. Earlier (p,t) reaction studies of both ^{166}Er [32] and ^{168}Er [33,36] showed important differences in the population strengths of the lowest excited 0^+ states (up to about 2 MeV excitation). Actually, both ^{166}Er and ^{168}Er showed up as anomalous cases among the rare-earth nuclei in studies that considered different properties of the 0^+ states. Thus, in connection with the γ-decay properties of the 0^+_2 state [17,20] ^{166}Er (and maybe ^{164}Er too) has an anomalous behavior [37,38]. Also, the nucleus ^{168}Er appeared as unique among the many rare-earth nuclei between ^{152}Gd and ^{190}Os studied with the (p,t) reaction [2], because up to about 2.5 MeV the $2n$-transfer strength to 0^+ states is fragmented into several small components, while more significant strength is found in a group of levels with energy between 2.5 and 3.0 MeV, a behavior that remained unexplained.

In view of these differences between the two neighboring Er isotopes, it was considered worth to investigate ^{166}Er with a high-resolution (p,t) reaction experiment, up to higher excitation energies. To this end, an experiment similar to that of Ref. [4] was performed, with the ^{168}Er$(p,t)^{166}$Er reaction at an incident energy of 25.0 MeV. Section II describes this experiment and its results, and Sec. III presents a discussion of these results.

II. EXPERIMENTAL

A. Measurements

The experiment was performed with a proton beam of 25.0 MeV delivered by the Tandem accelerator of the Meier

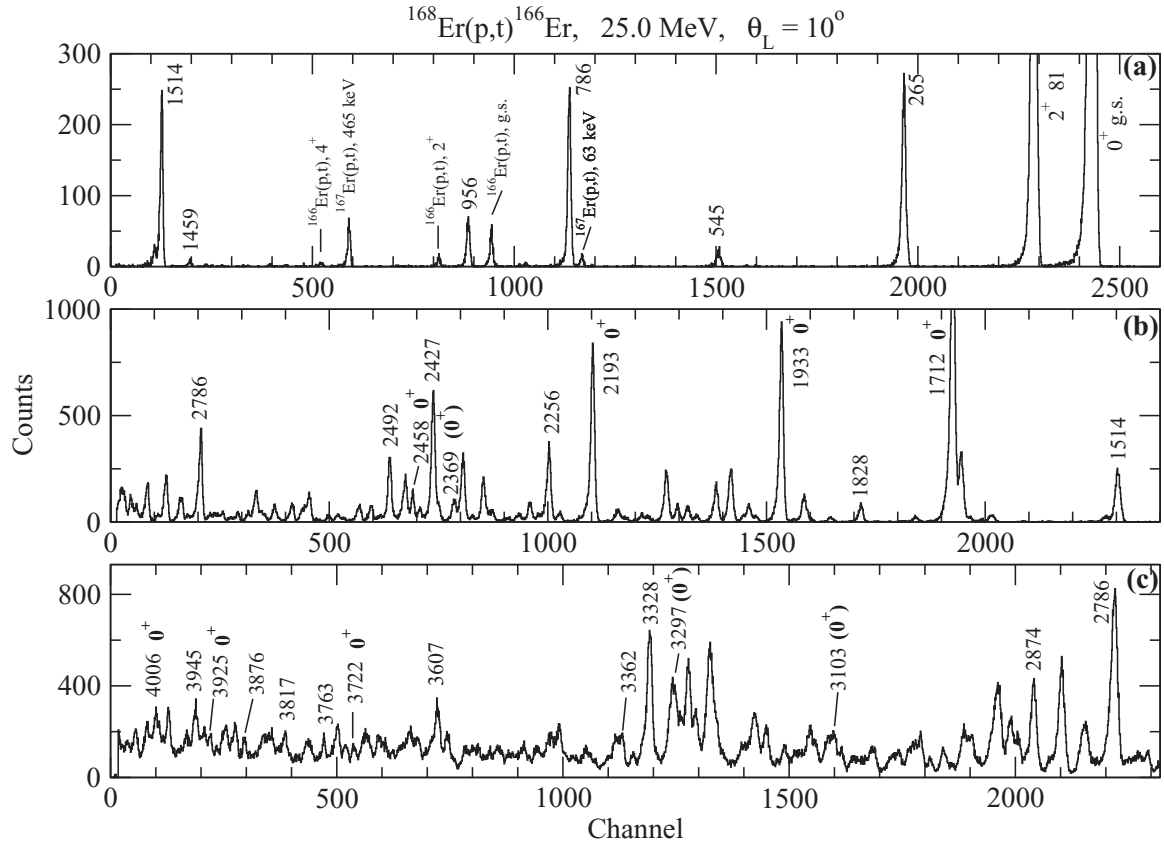

FIG. 1. Spectra measured at an angle $\theta_L = 10^\circ$ for the ^{168}Er$(p,t)^{166}$Er reaction at 25.0 MeV. The three spectra shown have been measured for three different magnetic field settings of the Q3D spectrograph, and integrated charges of (a) 2.8, (b) 4.7, and (c) 10.1 mC, respectively. Peak labels represent excitation energies in keV. The states assigned as 0^+ are marked.

Leibnitz Laboratory of the University and Technical University in Munich. The conditions were similar to our previous study of the ^{170}Er$(p,t)^{168}$Er reaction [4]. The target was 98% enriched in ^{168}Er, had a thickness of 120 μg/cm^2, and was deposited on a 13 μg/cm^2 Carbon backing. The most important impurities in the target were ^{166}Er and ^{167}Er (about 1% each).

The reaction products were analyzed with the Munich Q3D spectrograph [39], and then detected in a 1 m long cathode strip focal plane detector [40,41], which made ΔE-$E_{\rm rest}$ particle identification and position determination. The acceptance of the spectrograph was 12.8 msr ($\pm$21 mm $\times$ $\pm$24.5 mm horizontal/vertical), except for the most forward angle (5°) where it was 6.0 msr ($\pm$10 mm $\times$ $\pm$ 24.5 mm horizontal/vertical). Beam currents during the measurements were between 0.5 μA and 1.8 μA.

Spectra were measured at seven angles: 5°, 10°, 14°, 17.5°, 23°, 30°, and 37.5°. For each angle, three spectra were collected, with three different magnetic settings of the spectrograph, such as to cover the excitation energy range from 0 to $\approx$ 4.1 MeV, the magnetic field values being chosen in such a way that these runs have overlaps in energy. The energy calibration was performed using the reactions ^{154}Gd$(p,t)^{152}$Gd [2], ^{172}Yb$(p,t)^{170}$Yb [5], and ^{208}Pb(p,t) [42] under the same magnetic settings. The different angle runs were normalized to the beam current integrated into a Faraday cup placed behind the target.

Figure 1 shows the spectra measured with the three magnetic settings at the laboratory angle of 10°. A FWHM energy resolution of about 5 keV was obtained for the whole measured energy range. The spectra were practically background free. Peaks due to the two target impurities were seen only in the spectrum of the first magnetic setting. Under these conditions, more than 140 excited states were observed in ^{166}Er up to 4.07 MeV excitation, and angular distributions could be determined for most of them.

B. Results

The 0^+ states are the easiest to assign because their angular distributions in the (p,t) reaction, with a $L = 0$ transfer, have a strong peak at 0°. The assignment of the $L = 0$ character was generally based on an analysis with DWBA-calculated cross sections. Table I presents information on the 0^+ states both known before [16] and assigned in the present work. At this beam energy, and for this mass region, the 0^+ assignment was based, in many cases when the angular distribution was known only for a few angles, on the ratio $R = \sigma(5^\circ)/\sigma(17.5^\circ)$. The criterion $R > 3.0$ was considered as rather safe to distinguish the $L = 0$ from the $L > 0$ cases [2,5–8]. The R quantity is also given in Table I.

The DWBA calculations are similar to those presented in Ref. [4]. They were performed with the code CHUCK3 [43],

TABLE I. 0^+ states of ^{166}Er observed in the present experiment. Tentative 0^+ assignments are indicated by excitation energy values placed within parentheses (see Fig. 2 and explanations in text).

ENSDF Ref. [16] (keV)	$(n, n'\gamma)$ Ref. [20,21] (keV)	(t, p) Ref. [32] (keV)	(p, t) Ref. [32] (keV)	Present experiment E_x (keV)	$d\sigma/d\Omega(5^\circ)$ [μb/sr]	R [$\sigma(5^\circ)/\sigma(17.5^\circ)$]	Relative strength
0	0	0	0	0	1527(16)	60.6(15)	100
1460.031(6)	1459.9	1460(1)	1458(2)	1458.3(6)[a]	0.77(15)	0.50(11)	–
1713.4(7)	1713.4	1714(2)	1713(1)	1711.7(10)	333(4)	47.0(21)	12.7
1934.1(5)	1934.4	–	1935(2)	1933.1(10)	150(1)	42.2(21)	6.4
1942.6(4)	1942.7	–	–	–	–	–	–
2187		2197(3)	2196(2)	2193.5(10)	129(1)	33.8(18)	5.4
				[2369.1(10)]	7.9(4)	6.4(10)[b]	0.31
				2457.8(15)	17.9(5)	18.2(36)	0.68
				[3103.1(15)]	7.0(3)	4.1(7)[c]	0.26
				[3296.6(15)]	20.6(5)	4.9(4)	0.66
				3721.7(15)	2.1(2)	6.4(24)	0.07
				3924.9(15)	3.1(2)	7.5(27)	0.10
				4005.6(15)	5.4(4)	5.5(9)	0.19

[a]The peak observed at 1458.2 keV does not show an $L = 0$ component (see the R ratio in the seventh column and the angular distribution in Fig. 2). Thus, it mainly corresponds to the $(2)^-$ state at 1458.1 keV [16,22,27,29,45], while the 0^+ state at 1460 keV, observed in several other experiments [16,32], is very weakly populated in our experiment.
[b]ratio $\sigma(5^\circ)/\sigma(10^\circ)$.
[c]ratio $\sigma(5^\circ)/\sigma(14^\circ)$.

using optical model parameters from Ref. [44]. These calculations use a semimicroscopic form factor, which assumes that the pair of transferred neutrons originates from the available occupied shell model orbitals (n, l, j). For the natural parity states J^π in the final nucleus, $J = L$ and $\pi = (-1)^L$, and the pairs of transferred neutrons are expected to be based on the $1h_{9/2}$, $1i_{13/2}$, $2f_{7/2}$, $2f_{5/2}$, and $3p_{3/2}$ orbitals. The shape of the one-step DWBA-calculated angular distributions depends only slightly on the transferred neutron configuration (j^2).

Figure 2 presents a comparison between the experimental angular distributions and those calculated with DWBA, for the states assigned as 0^+. Because (i) the shape differences between calculations with different j^2 configurations are not big, (ii) we do not know the microscopic structure of the states, and (iii) sometimes we miss experimental points at some angles, the calculated curves in Fig. 2 (normalized to the experimental points) correspond to the same configuration transfer, $f^2_{7/2}$, as in Ref. [4]. The 1460 keV state (Table I) deserves a special comment. We observe a peak with excitation energy of 1458.3 keV, that was assigned to the doublet of states 1458.2 keV, (2^-) and 1460.0 keV, 0^+. The 1458.2 keV state was clearly seen in ^{166}Tm ϵ decay [45], in $(n, n'\gamma)$ [22], in (^{3}He, d) and (α, t) reactions [27,29], and (d, t) and (^{3}He, α) [29] and therefore its presence cannot be questioned. The 1460 keV state was clearly seen in the (t, p) reaction [32], and possibly, with a very small intensity (less than 0.25% from that of the gs $\rightarrow$ gs transition) in the (p, t) reaction [32]. Our 1458 keV peak does not show a sizable contribution from the 0^+ state (Figs. 1 and 2), its angular distribution being reasonably well reproduced by a DWBA transfer to the unnatural parity state 2^- (Fig. 2). Therefore the 0^+ state at 1460 keV is very weakly excited, if at all, in our (p, t) experiment. The 1943 keV state, thoroughly studied and assigned as the two-γ-phonon state in Ref. [21] and adopted as (0^+) in ENSDF [16] was not seen in this experiment. In summary, besides the five excited 0^+ states known up to 2.2 MeV, we have observed up to 4.0 MeV excitation other seven 0^+ states (three of them only tentatively assigned as 0^+), as shown in Table I and Fig. 2. In total, up to 4.0 MeV there are about 12 excited 0^+ states, compared to about 25 in ^{168}Er [4]. A few other states found with the R ratio around 3.0 were not assigned as 0^+ candidates because their angular distribution either lacked important points (angles), or the DWBA description was not sufficiently good.

Figure 3 and Table II present the states either previously known as 2^+, or assigned in this work as 2^+. Most of these states are reasonably well described by the DWBA (one-step process) calculations, having a typical shape, which peaks around 16°. Coupled channel (CC) calculations were needed in order to describe the shapes observed for the angular distributions of the 2^+ states known at 80 and 786 keV. For the CC calculations, both for these 2^+ states and states of other spins, only two different coupling schemes were considered, *m1a* and *m2a* in the notations of Ref. [46]. The strength parameters of the couplings between different channels were chosen such as to reproduce the observed angular distributions. Up to 4.0 MeV excitation, 39 states have been assigned as 2^+.

Other transfers, with L different from 0 or 2 could be assigned to a number of states as shown in Fig. 4. The two known lowest 4^+ states (at 265 and 957 keV) and 6^+ states (at 545 and 1216 keV) show angular distribution shapes that could be described only by CC calculations. This was also the case for some other states (Fig. 4), although not in all cases one could make unambiguous assignments.

As explained in Sec. III A, in assigning transferred L values we neglect small differences in shape of the DWBA curves

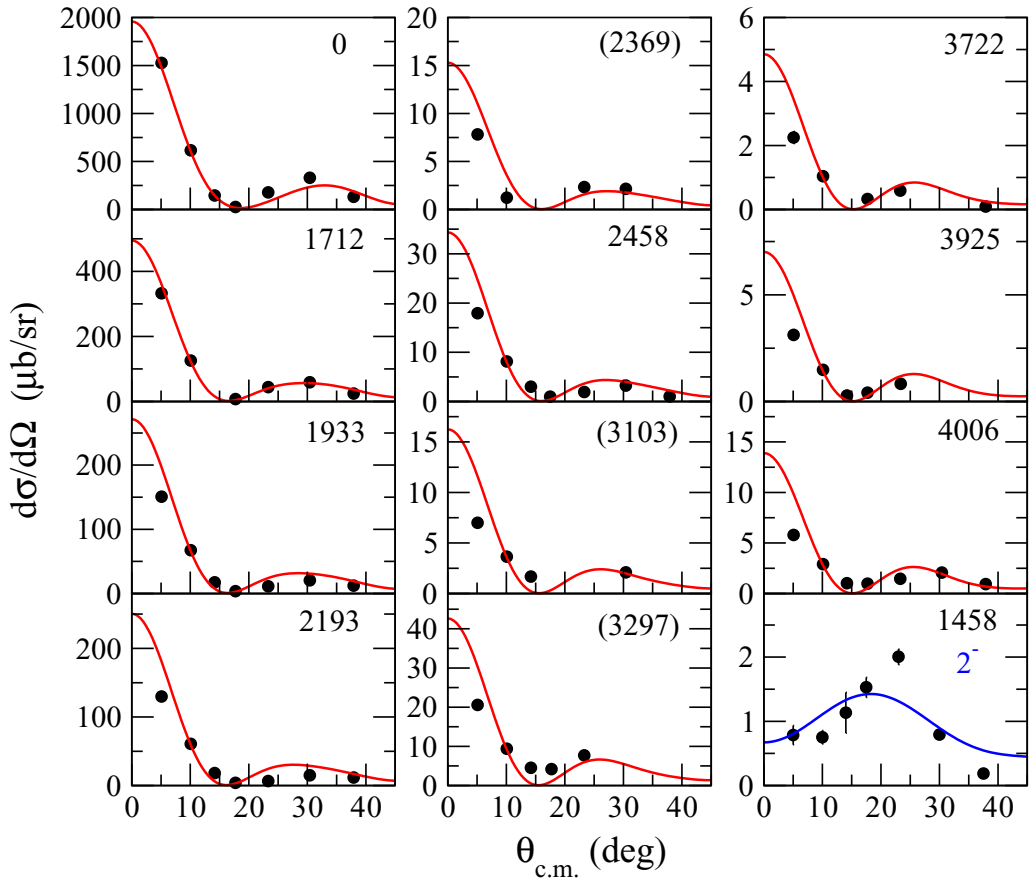

FIG. 2. Angular distributions of states assigned as 0^+. The curves are DWBA calculations normalized to the data (see text). The angular distribution observed for the 1458 keV peak (lowest right side graph) is well described by a one-step DWBA calculation for a 2^- transfer, as required by the $(2)^-$ state known at 1458 keV [16,22,27,29,45], therefore the known 1460 keV 0^+ state [16,32] has a negligible population in our reaction. For the states with excitation energy given within parentheses the $L = 0$ assignment is tentative because of the smaller number of points.

corresponding to different $(j_1 j_2)$ transfers, and use DWBA curves calculated with the same form factor, but for the Q value corresponding to each particular state. By normalizing the calculated cross section (which is corrected for the Q value) to the experimental one, one gets a normalization factor, which characterizes the $2n$-transfer strength for each state. If the DWBA calculated shape describes reasonably well the experimental one, the relative normalization factors are close to the relative angle-integrated cross sections, both these quantities showing how the (p, t) reaction strength is distributed over different states [4]. The relative $2n$-transfer strengths for the 0^+ and 2^+ states are given in Tables I and II.

Summarizing, we observed in the present study about 140 excited states, and, on the basis of their angular distributions one could confirm or propose spin-parity values to almost 90 excited states. All these states are summarized in Table III, where previously known states as adopted in ENSDF [16] are also given if the difference in energy to those observed in our experiment is within about 3 keV. One should emphasize that, in certain cases when the excitation energies match within this range, the two levels may not necessarily be the same. The energy of a state observed in the present experiment has been listed in Table III if the corresponding peak was observed at a minimum of four angles. For a number of about 60 of the observed states one could not make a definite assignment of the transferred L value, either because of missing points at certain angles of the angular distribution, or due to assignment ambiguities. The peaks observed at 1663 keV and 2241 keV contain contributions from two unresolved, previously known states (Table III and Fig. 4).

III. DISCUSSION

A. General considerations

The large number of excited 0^+ states found in rare-earth nuclei may be due to different excitation mechanisms, such as: β vibrations (due to the residual quadrupole interactions) [47], usually expected to appear within the pairing gap; pairing vibrations (due to the residual pairing interactions) that should appear above the pairing gap [48]; multiphonon excitations based on both positive and negative parity vibrational modes (such as 2β, 2γ, double octupole, etc.); spin-quadrupole interaction excitations [49]; shape coexistence (in regions of changing of the equilibrium deformation); etc. In the two-neutron transfer reactions the transition strengths are sensitive to correlations in the transferred nucleon pair and in principle

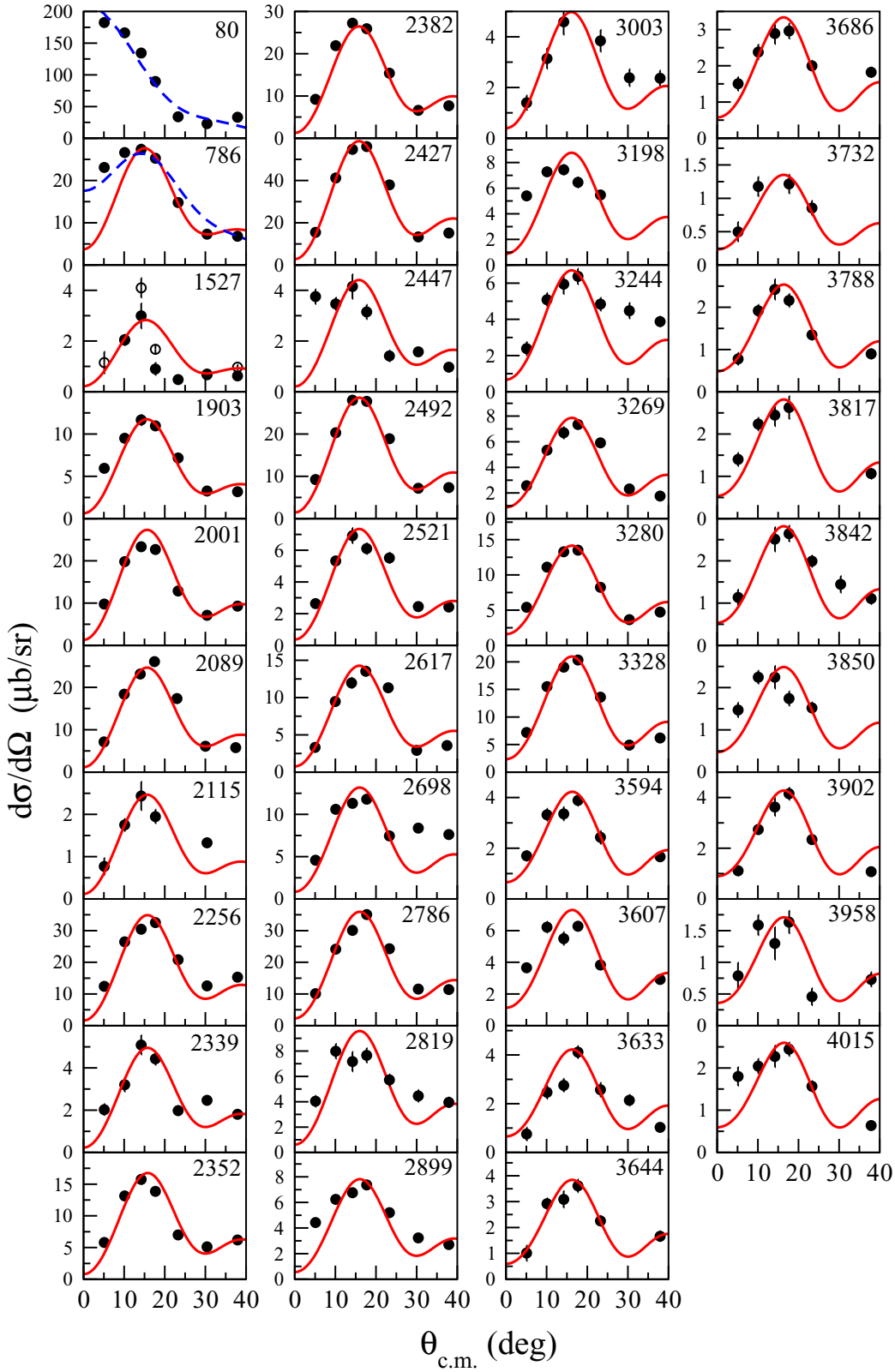

FIG. 3. Angular distributions of 2^+ states. The level at 1527 keV was seen in the spectra collected with both the first and second magnetic setting (there is a small region of overlap between the two settings). The open and filled symbols are the cross sections calculated for the spectra of the two settings, respectively. In all the other cases, the states have been seen at only one magnetic setting and only full symbols are given. The continuous (red) curves represent DWBA (one-step process) calculations normalized to the experimental data, while the dashed (blue) curves are coupled-channel calculations (see text).

TABLE II. 2^+ states of ^{166}Er observed in the present study (see also Fig. 3). Tentative assignments are indicated by parentheses. Only the states at 80, 786, and 1527 keV were known before with firm 2^+ assignments [16].

E_x (keV)	$\frac{d\sigma}{d\Omega}(14^\circ)$ $(\frac{\mu b}{sr})$	Relative strength	E_x (keV)	$\frac{d\sigma}{d\Omega}(14^\circ)$ $(\frac{\mu b}{sr})$	Relative strength
80.4(2)	134.2 (25)	100	786.0(1)	27.4 (11)	18.2
1526.8(8)	3.0 (5)	1.5	1903.2(15)	11.6 (6)	5.4
2001.1(10)	23.3 (8)	12.1	2089.4(10)	23.1 (8)	10.9
2115.0(15)	2.4 (3)	1.1	2256.3(10)	30.4 (9)	14.7
2338.8(10)	5.1 (5)	2.1	2351.9(10)	15.7 (7)	6.9
2382.3(10)	27.2 (9)	10.9	2426.7(10)	54.7 (13)	24.2
[2446.9(15)]	4.1 (3)	1.8	2492.4(15)	28.0 (9)	11.5
2520.9(15)	6.9 (5)	3.0	2616.9(15)	11.9 (7)	5.6
2698.0(15)	11.3 (4)	5.0	2786.3(15)	31.4 (11)	13.6
2818.7(15)	7.2 (8)	3.6	2899.2(20)	6.7 (4)	2.9
3002.7(15)	4.6 (5)	1.8	[3198.0(15)]	7.4 (5)	3.1
3244.4(15)	5.9 (5)	2.3	3269.4(15)	6.7 (5)	2.7
3280.1(15)	13.3 (6)	4.9	3327.6(15)	19.0 (6)	7.3
3594.2(15)	3.4 (3)	1.4	3606.8(15)	5.5 (4)	2.4
3633.4(15)	2.8 (3)	1.4	3643.6(15)	3.1(3)	1.3
3686.5(15)	2.9 (3)	1.1	3731.6(15)	∼1.2	0.4
3787.8(15)	2.4 (3)	0.82	3817.1(15)	2.4 (3)	0.91
3842.2(15)	2.5 (3)	0.91	[3849.6(15)]	2.2 (3)	0.8
3901.6(15)	3.6 (3)	1.4	3957.8(15)	1.3 (3)	0.55
4015.0(15)	2.2 (3)	0.82			

provide information about the nature of the populated states [50].

Experimentally, assignment of observed 0^+ states to different such excitation types constitutes an intricate task, and actually requires extended information obtained from more than one experiment. In ^{166}Er there are several experiments dedicated to the study of the structure of the lowest excited 0^+ states. Actually, the observation of all known such states up to about 2 MeV excitation was based on data obtained in more than one experiment (see Table I). Thus, the 0_2^+ state at 1460 keV state (Table I) was clearly seen in the (t, p) reaction [32] and is extremely weakly excited in the (p, t) reaction ([32] and the present work) and in inelastic scattering [25]. It was well populated in the $(n, n'\gamma)$ reaction [20]. The 0_5^+ state at 1943 keV (Table I) was not observed in the present experiment and deserves a separate discussion. This level was only seen in the $(n, n'\gamma)$ study [21] and in the Coulomb excitation reactions of Refs. [26], while the evaluated database indicates a tentative 0^+ spin-parity assignment for this state [16]. In our experiment, this level should be located on the tail of the much larger peak at 1934 keV (only 9 keV apart) but its cross section is small enough that it is completely obscured by the high-energy tail of the 1934 keV peak. Furthermore, one phonon states are expected to be populated with a low cross section [51] and the multiphonon states should be even weaker, therefore, the nonobservation of this state might support the interpretation of this excitation as a 2γ-phonon state. The other states, up to 0_6^+ at 2.19 MeV were seen in different reactions (see Table I).

The first few excited 0^+ states in ^{166}Er together with the first two 2^+ states are shown in Fig. 5. These levels have been populated in the present experiment and the previous ones [16]. The figure summarizes the information concerning the (p, t) transfer strength (width of the horizontal lines), the reduced decay strength (width of the vertical arrows), and the nature of the 0^+ states. The 0_2^+, 1460 keV and 0_3^+, 1713 keV states decay towards the 2_1^+ and 2_2^+ (the γ-band head) states with small $B(E2)$ transition rates (of 1–2 W.u.), therefore their nature is noncollective and they were suggested as pairtype excitations [20]. On the other hand, the 0_4^+, 1934 keV state decays only to the 2_1^+ state by a 8.8 W.u. $E2$ transition, therefore it was assigned as the β-vibration state [20]. The 0_5^+, 1943 keV state was found to decay only to the 2_γ^+ state by a strong $E2$ transition of 21 W.u, and was assigned as the 2γ-phonon state [21]. Thus, combining various information on the 0^+ states, such as the pattern of their population in different reactions and decays and their electromagnetic decay properties allows possible assignments to different nuclear structure excitation paradigms. A unitary explanation of all these states would require advanced microscopic models, which take into account many degrees of freedom. Such models should be able to explain both the number of observed 0^+ states and the observed pattern of their population in two-neutron transfer reactions.

B. Two-neutron transfer strengths

Figure 6 shows the present information on the first few excited 0^+ states (up to about 2.5 MeV excitation) in Er isotopes, with emphasis on the two-neutron transfer strengths in the reactions (p, t) and (t, p), respectively [4,32,33,35,36]. One observes important differences between the two neighboring isotopes. In both ^{166}Er and ^{168}Er nuclei the first few excited states are appreciably populated in the (t, p) reaction, cumulating a strength of almost 30% from that of the ground state to ground state (gs → gs) transition [Fig. 6(a)], also seen

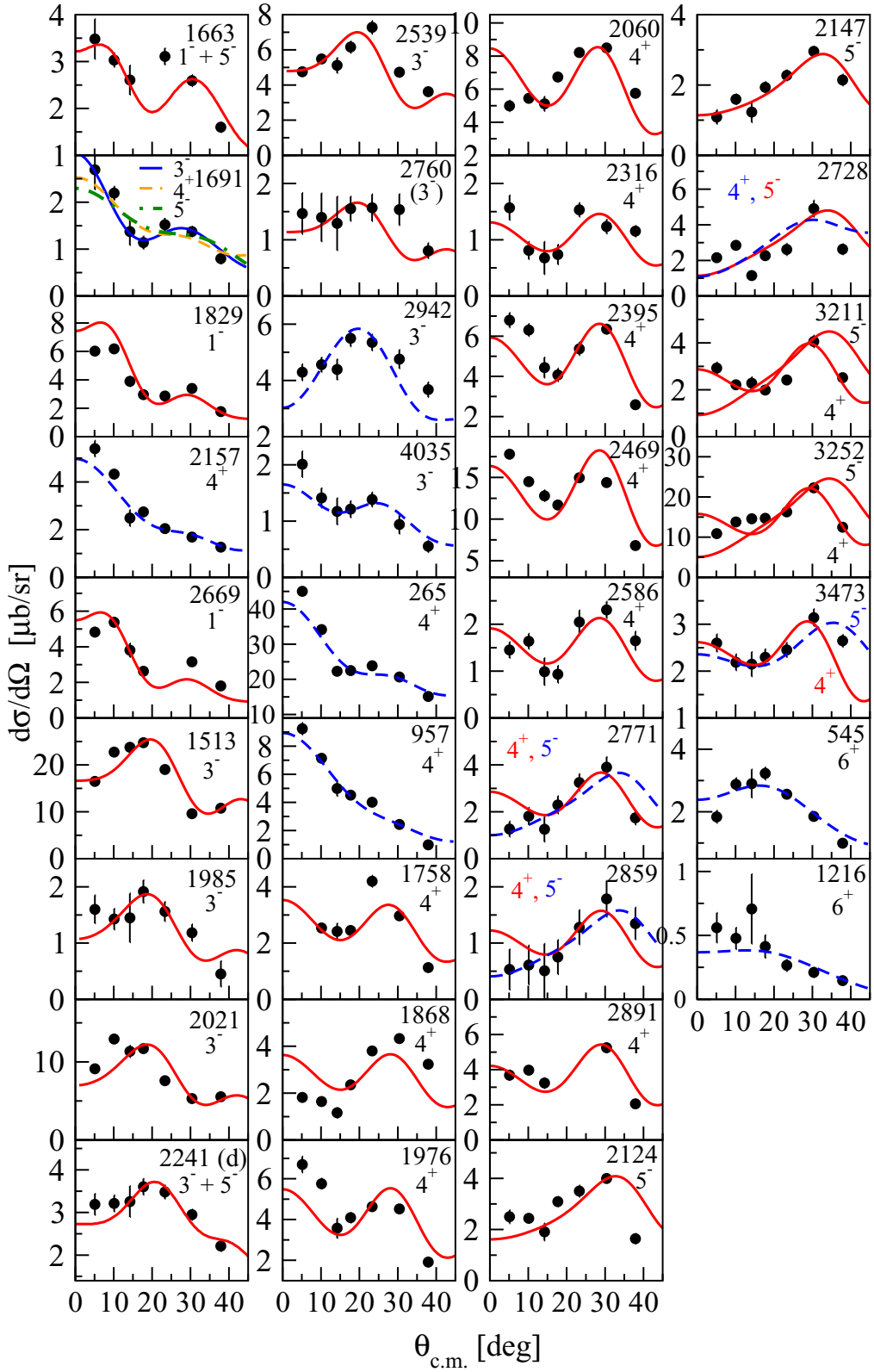

FIG. 4. Transferred L values, other than 0 or 2, assigned to excited states in ^{166}Er. The continuous (red) curves are one-step DWBA calculations normalized to the data, and the dashed (blue) curves are coupled-channel calculations (see text). The peaks with excitation energies of 1663 and 2241 correspond to unresolved doublets with known spin/parity, as shown both in this figure and in Table III.

TABLE III. Complete list with energy and spin assignment for the levels of ^{166}Er, as observed in the present experiment in comparison with the known excitations in the ENSDF database [16]. Previously known states with spin up to $6\hbar$ are shown only if the differences in the excitation energy are below about 3 keV. The states marked with a star (∗) are from ref. [22], as adopted in the XUNDL database [23]. The matching of the excitation energies within this range does not always imply, however, that the two levels are the same. Cross sections of the present (p, t) reaction are also given, as follows: for the 0^+ levels, at the angle of 5°; 1^-–assigned states: at 10°; 2^+: at 14°; 3^- and 4^+: at 17.5°; 5^- and 6^+: at 23°; other states (spin not assigned): at 10°. The experimental uncertainties given in the table are statistical only, for both energy and cross section.

ENSDF [16]		Present expt.		
E_x (keV)	J^π	E_x (keV)	J^π	$\frac{d\sigma}{d\Omega}$ ($\frac{\mu b}{sr}$)
0.0	0^+	0.0	0^+	1527 (16)
80.5776(20)	2^+	80.4(2)	2^+	134 (3)
264.990(3)	4^+	264.9(2)	4^+	22.5 (5)
545.454(4)	6^+	545.0(3)	6^+	2.6 (1)
785.905(6)	2^+	786.0(1)	2^+	27.4 (11)
956.232(5)	4^+	956.8(4)	(4^+)	4.5 (3)
1215.968(5)	6^+	1216.7(8)	(6^+)	0.3 (1)
1458.154(9)	$(2)^-$	1458.3(6)		0.8 (2)
1513.751(9)	3^-	1513.2(6)	3^-	24.7 (4)
1528.401(10)	2^+	1526.8(8)	2^+	3.0 (5)
1662.435(5)	1^-			
		1663.0(8)	$1^- + 5^-$	2.6 (3)
1665.799(6)	$5^{(-)}$			
1678.765(24)	$(4)^+$	1676.9(8)		0.7 (2)
1692.297(5)	5^-	1690.8(10)	$(3^-, 4^+, 5^-)$	2.2 (2)
1703.050(18)	$(2, 3, 4)^+$	1701.1(10)		28.4 (5)
1713.4(7)	0^+	1711.7(10)	0^+	333 (4)
1760.64(15)∗	4^+	1758.0(10)	4^+	2.4 (3)
1830.425(12)	1^-	1828.6(10)	1^-	6.2 (2)
1865.17(4)		1867.8(15)	4^+	2.3 (2)
1897.27(10)	(6^+)	1896.2(10)		1.9 (2)
1904.8(5) ?	2,3,4	1903.2(15)	2^+	11.6 (6)
1934.1(5)	0^+	1933.1(10)	0^+	150 (1)
1942.6(4)	(0^+)			
1969.71(17)	(2,3,4)	1967.4(10)		1.9 (2)
1978.422(13)	4^+	1976.6(10)	4^+	4.1 (3)
1985.629(12)	3^-	1984.6(10)	3^-	1.9 (2)
2001.865(12)	$(3)^-$	2001.1(10)	2^+	23.3 (8)
2021.348(12)	$(2, 3)^-$	2021.0(10)	3^-	11.7 (3)
2046.87(4)	$2^+, 3^+$	2047.9(10)		0.4 (2)
2062.1(17)		2060.1(10)	4^+	6.7 (3)
2074	(2^-)	2074.3(10)		5.0 (2)
		2089.4(10)	2^+	23.1(8)
2116	(6^+)	2115.0(10)	2^+	2.4 (3)
2124.7(7)	(5^-)	2124.1(15)	5^-	3.5 (2)
2148.6(5)	(4^-)	2147.6(15)	5^-	2.3 (2)
2155.8(7)	(6^+)	2157.4(15)	4^+	4.3 (2)
2196.3(17)	0^+	2193.5(10)	0^+	129 (1)
2240.1(10)	(5^-)			
		2240.9(15)	$3^- + 5^-$	3.6 (2)
2243.087(20)	3^-			
		2256.3(10)	2^+	30.4 (9)
2273.01(3)	3^-	2272.0(15)		1.5 (2)
2282.68(5)	$2^{(+)}, 3$	2283.8(10)		14.2 (4)
2302(3)		2300.0(15)		2.3 (2)
2315	$(3, 4)^+$	2316.0(10)	4^+	0.7 (2)
		2338.8(10)	2^+	5.1 (5)
2352.91(8)	$2^{(+)}, 3$	2351.9(10)	2^+	15.7 (7)
		2369.1(10)	(0^+)	7.9 (4)
2382.26(4)	$(3)^+$	2382.3(10)	2^+	27.2 (9)
2394.50(10)∗		2395.4(15)	4^+	4.1(3)
		2418.7(15)		5.1 (4)
2427		2426.7(10)	2^+	54.7 (13)
2444.16(24)		2446.9(15)	(2^+)	4.1 (3)
		2457.8(15)	0^+	17.9 (5)
		2469.2(15)	4^+	11.7 (4)
		2492.4(15)	2^+	28.0 (9)
		2520.9(15)	2^+	6.9 (5)
2538.89(14)∗	3^+	2539.4(15)	3^-	6.2 (3)
2563	6^+	2563.5(15)		1.5 (2)
2586.06(12)	$(3, 4)^+$	2586.2(15)	4^+	1.0 (3)
		2616.9(15)	2^+	11.9 (7)
2624.8(3)	$(1, 2^+)$	2626.5(15)		4.0 (3)
2632.66(17)	$(3, 4)^+$	2632.2(15)		1.7 (2)
		2642.5(15)		6.2 (2)
2671.98(17)		2668.6(15)	(1^-)	5.4 (3)
2687		2687.0(15)		3.1 (2)
		2698.0(15)	2^+	11.3 (4)
		2710.9(15)		2.3 (2)
2729.090(17)	$(3, 4)^+$	2728.4(20)	$(4^+, 5^-)$	2.6 (3)
2742		2739.0(15)		1.1 (2)
		2750.4(20)		1.7 (4)
		2759.8(20)	(3^-)	1.5 (2)
		2771.3(20)	$(4^+, 5^-)$	2.3 (4)
		2786.3(15)	2^+	31.4 (11)
		2818.7(15)	2^+	7.2 (8)
		2842.8(15)		13.9 (3)
2858.16(18)	$(1, 2)^+$	2859.0(15)	$(4^+, 5^-)$	0.8 (3)
		2873.5(15)		11.5 (3)
		2890.6(20)	4^+	3.3 (3)
		2899.2(20)	2^+	6.7 (4)
2912		2911.6(20)		11.7 (4)
		2921.2(20)		2.8 (4)
		2942.7(20)	3^-	5.5 (3)
		2951.7(15)		4.7 (3)
		2974.1(15)		2.4 (2)
		2991.4(15)		1.2 (2)
3000		3002.7(15)	2^+	4.6 (5)
		3011.5(15)		3.2 (4)
		3030.2(15)		2.5 (2)
		3058.2(15)		2.9 (2)
		3069.9(15)		1.2 (1)
		3079.0(15)		1.3 (1)
		3093.7(15)		1.6 (2)
		3103.1(15)	(0^+)	7.0 (3)
		3112.1(15)		2.9 (3)
		3124.7(15)		2.4 (2)
		3133.4(15)		4.0 (3)
3147		3144.8(15)		1.9 (2)

TABLE III. (*Continued.*)

ENSDF [16]		Present expt.		
E_x (keV)	J^π	E_x (keV)	J^π	$\frac{d\sigma}{d\Omega}$ ($\frac{\mu b}{sr}$)
3160		3162.3(15)		2.0 (2)
		3184.7(15)		5.0 (2)
		3198.0(15)	(2^+)	7.4 (5)
3211		3211.7(15)	$(4^+, 5^-)$	2.4 (3)
		3244.4(15)	(2^+)	5.9 (5)
3253		3252.8(15)	$(4^+, 5^-)$	16.3 (4)
		3269.4(15)	2^+	6.7 (5)
		3280.1(15)	2^+	13.3 (6)
3296		3296.6(15)	(0^+)	20.6 (5)
		3327.6(15)	2^+	19.0 (6)
		3362.1(15)		6.3 (3)
		3407.1(15)		1.8 (2)
		3443.7(15)		3.7 (2)
		3473.7(15)	$(4^+, 5^-)$	2.5 (2)
		3492.1(15)		2.5 (2)
		3506.1(15)		1.6 (2)
		3524.4(15)		2.6 (2)
		3568.7(15)		2.4 (2)
		3594.2(15)	2^+	3.4 (3)
		3606.8(15)	2^+	5.5 (4)
		3618.5(15)		1.2 (3)
		3633.4(15)	2^+	2.8 (3)
		3643.6(15)	2^+	3.1 (3)
		3654.3(15)		1.0 (2)
		3677.0(15)		1.6 (2)
		3686.5(15)	2^+	2.9 (3)
		3701.4(15)		1.9 (3)
		3706.9(15)		1.9 (3)
3721		3721.7(15)	0^+	2.1 (2)
		3731.6(15)	2^+	∼1.2
		3744.2(15)		3.1 (2)
		3763.6(15)		1.4 (2)
		3787.8(15)	2^+	2.4 (3)
		3817.1(15)	2^+	2.4 (3)
		3842.2(15)	2^+	2.5 (3)
		3849.6(15)	(2^+)	2.2 (3)
		3876.0(15)		1.2 (2)
		3901.6(15)	2^+	3.6 (3)
		3924.9(15)	0^+	3.1 (2)
3932		3932.6(15)		2.1 (2)
		3945.4(15)		4.3 (2)
		3957.8(15)	2^+	1.3 (3)
		3986.1(15)		3.2 (2)
		3999.5(15)		1.5 (2)
		4005.6(15)	0^+	5.4 (4)
		4015.0(15)	2^+	2.2 (3)
		4035.0(15)	3^-	1.2 (2)

in the lower graphs [Figs. 6(f) and 6(g)] showing three 0^+ states with relatively large strengths (above several percent) in each nucleus. On the other hand, the (p, t) reaction populates rather differently 0^+ states in the two nuclei. In ^{166}Er the states at 1490 keV (0_2^+) and 1943 keV (0_5^+) are practically not populated, but there are other three strongly populated states

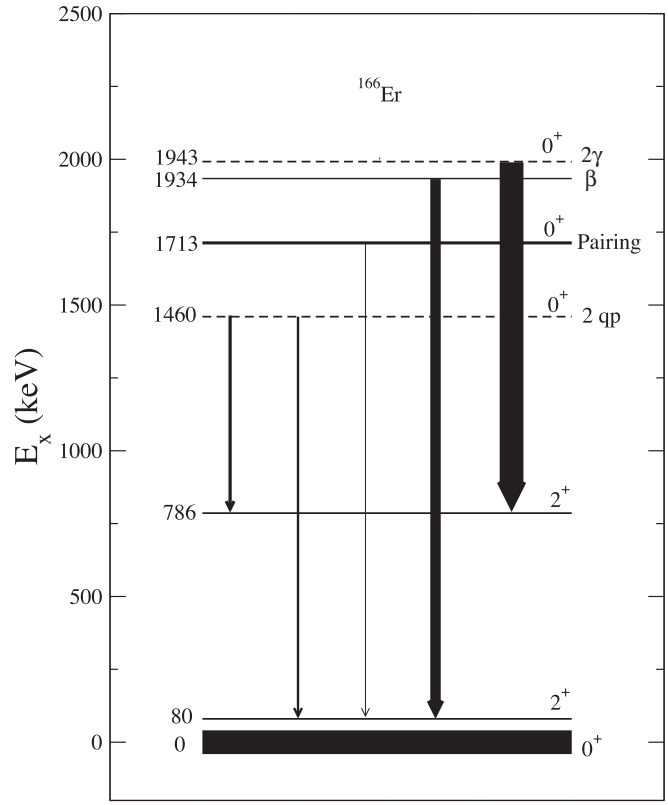

FIG. 5. Partial low-lying level scheme of ^{166}Er. The width of the horizontal lines is proportional with the (p, t) transfer strength, while the width of the arrows is proportional to the reduced transition probabilities. The dashed lines represent states, which were not seen in the present study. The nature of the 0^+ states as deduced from all available experimental data is also shown.

up to about 2 MeV excitation, while in ^{168}Er the population of all low-lying 0^+ states in the same energy range is much weaker, around 1% or less [Figs. 6(b), 6(d) and 6(e)].

There are different mechanisms proposed to explain the population of excited 0^+ states in two-neutron transfer reactions. Thus, in the IBA-based approach of Ref. [54], the two-nucleon transfer cross sections to excited 0^+ states are correlated to the overall change in collective structure, as measured, e.g., by the change in the $R(4/2)$ ratio. The different excitation patterns of ^{166}Er and ^{168}Er (as shown by Fig. 6) cannot be explained in this way, because the changes in $R(4/2)$ from ^{164}Er to ^{170}Er are very small (smaller than 0.02 for two even-even neighboring isotopes).

On the other hand, in well-deformed nuclei such as in the rare-earth region, one expects that the $L = 0$ strength is found mainly in the gs → gs transition. Exceptions from this rule were found for the nuclei with $N = 108$ and $N = 98$ for which there are subshell closures in the Nilsson level diagram, comparable to the neutron pairing force strength. The proposed mechanism is that the deformed shell gap disrupts the coherent summing of transition amplitudes to the superconducting ground states, spreading $L = 0$ strength to excited 0^+ states (Ref. [32]). The existence of the $N = 98$

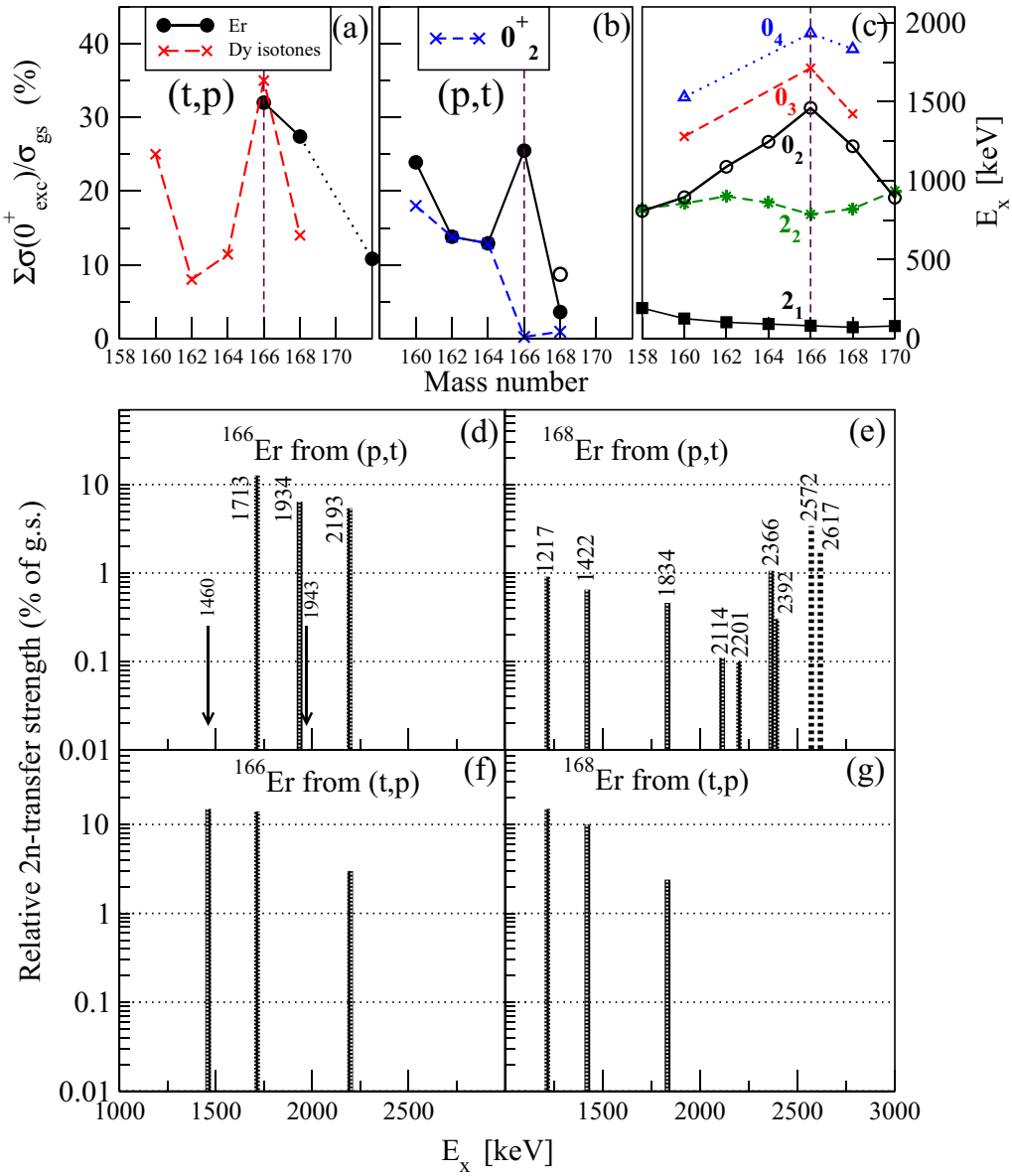

FIG. 6. Relative cross sections for 0^+ states of Er isotopes, populated in the (p, t) and (t, p) reactions. Graphs (a) and (b): summed strength for the excited 0^+ states known up to about 2.5 MeV, normalized to that of the gs $\rightarrow$ gs transition taken as 100 in the (t, p) and (p, t) reactions, respectively. Graph (c) shows the evolution of the excitation energy of some selected states. The lower four graphs show relative strengths for individual states, observed for ^{166}Er in the (d) (p, t) and (f) (t, p) reactions, and for ^{168}Er, graphs (e) and (g), respectively. Experimental data are from: ^{160}Er from (p, t): Ref. [35]; ^{162}Er from (p, t): [34]; ^{164}Er from (p, t): [34,36]; ^{166}Er from (p, t): Ref. [32] (intensities that fit those found in this work); ^{166}Er from (t, p): [32]; ^{168}Er from (p, t): [4]; ^{168}Er from (t, p): [33]; ^{172}Er from (t, p) [52]. The $\times$ symbols and dashed red line in graph (a) show the values for the (t, p) intensities in the isotonic Dy isotopes [53], while those in black are the corresponding values for Er isotopes; in panel (b), the summed transfer intensities are given in black, while in blue there are the intensities for the 0^+_2 state; the empty circle for ^{168}Er in graph (b) includes the two states just above 2.5 MeV; in (c) the black squares, green stars, empty circles, red crosses, and blue diamonds correspond to the 2^+_1, 2^+_2, 0^+_2, 0^+_3, and 0^+_4 states, respectively; the vertical dashed lines in (a)–(c) at mass 166 mark the $N = 98$ subshell closure; in panel (d), the arrows correspond to known 0^+ states, which were not observed in the present experiment. Note: the (t, p) reaction intensities correspond to cross sections measured at one angle [32,33,52].

subshell gap has been proposed by several theoretical studies that concentrated their attention on reproduction of the two-neutron transfer intensities [53,55]. This would explain the large (p, t) and (t, p) reaction strengths observed for the $N = 98$ nuclei ^{166}Er and ^{164}Dy [Figs. 6(a) and 6(b)]. In addition, more recent work showed that the subshell gap at $N = 98$ is a well established feature in the Nilsson diagram. For example, the gap was also established in the case of ^{167}Tm where its role in determining the nature of the alignment and its shape driving effect were emphasized [56]. Guided by these previous findings, we try in the following paragraph to have a closer look at several observables in the Er isotopic chain and the neighboring nuclei that might reveal discontinuities when studied systematically.

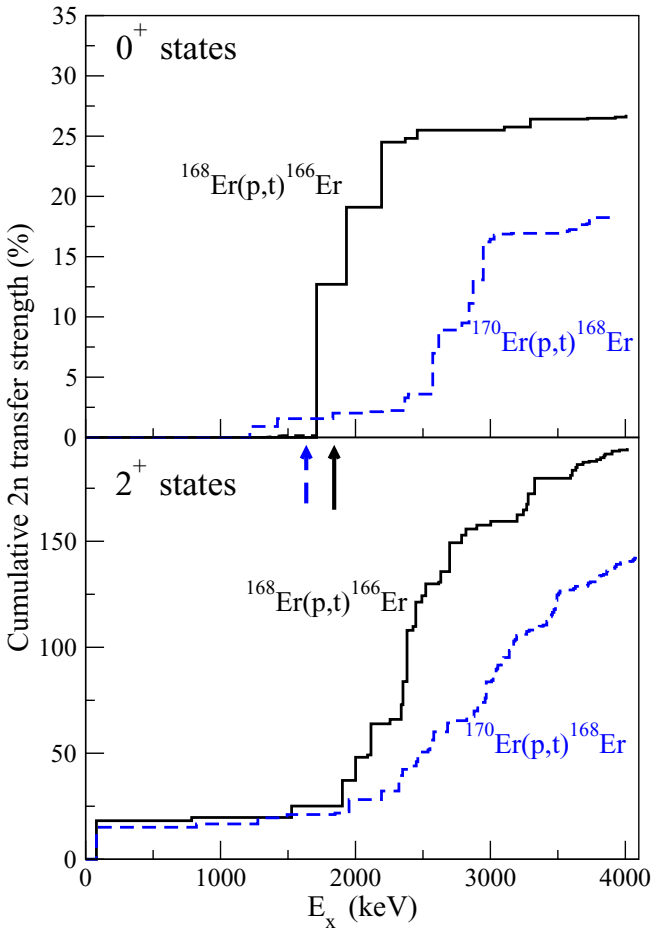

FIG. 7. Cumulative two-neutron transfer strengths in the (p,t) reaction. The arrows indicate the position of the pairing energies in the two nuclei.

Figure 6(c) shows that there is indeed an important change of structure at the deformed subshell closure $N = 98$: the evolution patterns of the excitation energies of both the 2_2^+ state, and of the first few excited 0^+ states display clear discontinuities (change of slope) at this neutron number. The structural changes at $N = 98$ also show another fact. The Er isotopes with N below 98 have a rather strong population of the 0_2^+ state in the (p,t) reaction, while in the isotopes with N equal to 98 and 100 the population of this state drops drastically [Fig. 6(b)]. It is more difficult to qualitatively understand the large (t,p) $2n$-transfer intensities also in the case of ^{168}Er nucleus [Fig. 6(a)].

A more detailed view of the differences in the population patterns of the 0^+ and 2^+ states of the two nuclei, in the (p,t) reaction, is given in Fig. 7, which displays the cumulative transfer strength as a function of the excitation energy. There is a significant population of the 0_3^+, 0_4^+, and 0_6^+ states in ^{166}Er, reaching 25% of the gs $\rightarrow$ gs strength at 2.2 MeV, after which much smaller strengths go into higher states, reaching about 27% around 4.0 MeV. In ^{168}Er, the lowest few 0^+ states do not exceed a total of 2.5% up to almost 2.5 MeV, and there is a stronger accumulation of transfer strength in the region 2.6–3.0 MeV. The population of the 2^+ states shows similar differences, with a steep increase around 2.4 MeV in ^{166}Er, and a gradual increase in ^{168}Er after about 2 MeV, the total strength at ~4 MeV being smaller than that of ^{166}Er. Naively, the shift towards higher excitation energy of the stronger $2n$-transfer strength in ^{168}Er may be attributed to states in which the extracted neutron pair comes from orbitals below the $N = 98$ subshell gap.

IV. COMPARISON TO MODEL PREDICTIONS

A. Microscopic models

Many previous studies considered the nature of the lowest 0^+ excited states. Thus, in the deformed nuclei, the 0_2^+ state was traditionally considered a collective excitation, such as the β vibration. However, the collective models were usually found to predict overestimated $B(E2)$ transition rates for the 0_2^+ states, indicating that they are less collective.

Within microscopic model studies, the 0^+ states are not assumed to be purely collective. Several such approaches were previously applied in the rare-earth region.

The first is the quasiparticle-phonon model (QPM) [57]. For the deformed nuclei, its Hamiltonian includes both monopole and quadrupole pairing, and a quadrupole-quadrupole force term. First extensive study was carried out in the case of ^{158}Gd [10], for which an increased number of 0^+ states was known [1]. The results showed that an appreciable number of 0^+ states are having an increased contribution of the two-octupole phonon component, in very good agreement with IBM calculations [9]. For the ^{168}Er nucleus, this model predicted that the lowest excited 0^+ states (up to about 3 MeV) are described as one-phonon excitations [4,11]. The microscopically generated phonons are generally built by several two-quasiparticle excitations, therefore they lack quadrupole collectivity. Two-phonon excitations appear at higher excitation energies. While the model predicts a large number of 0^+ states, it failed to reproduce in detail the distribution of the $2n$-transfer strength [4].

The second microscopic approach is the projected shell model (PSM), a truncated shell model with deformed bases [58]. The model was first applied to ^{158}Gd by adopting a restricted space spanned by two- and four-quasiparticle states [13]. The model produced very small $E2$ transition probabilities for the decay of the corresponding 0^+ states, indicating the need for introducing a mixing between the quasiparticle states and the collective degrees of freedom. Applied to ^{168}Er it also showed the relevance of two-quasiparticle configurations in the low-energy 0^+ states, although the calculated states contained less correlated linear combinations of two- and four-quasiparticle states than in the QPM approach [4]. The role of additional interactions such as the spin-quadrupole one, introduced in Ref. [49], on the 0^+ states, was studied in some deformed nuclei from this region [14,59].

More recent microscopic calculations have used the Hartree-Fock-Bogoliubov theory to map a five-dimensional collective quadrupole Hamiltonian and using the D1S Gogny interaction to study the global properties of nuclei across the nuclear chart in a systematic manner [60]. The results showed that in general the first excited 0^+ state is predicted at higher

excitation energy, and in the case of ^{166,168}Er, the band built on the 0_2^+ state does not correspond to the β vibration calculated with this model. Other two microscopic studies have been performed in the framework of the quasiparticle random-phase approximation (QRPA) [61,62]. The results agree that for the Er isotopes, only ^{170}Er can be considered as displaying characteristics of the β vibration for the first excited 0^+ state.

A more complex microscopic model is the generator coordinate method (GCM) [63]. It handles both shape vibrations (collective degrees of freedom) and single-particle degrees of freedom, therefore it can be applied not only to deformed nuclei, but also to soft and transitional ones. Thus, the GCM allows to investigate the role of all these degrees of freedom, and their coupling, in the most relevant low-lying structures (gsb, β, and γ bands) of large regions of nuclei. The GCM was recently applied to the Erbium isotopes $^{156-172}$Er, first in a version, which considered only axially symmetric shapes [64], and subsequently in an extended one, which took into account both deformation parameters (β, γ) [65]. These articles mainly concentrated on the detailed study of the 0_2^+ state. The evolution of the experimental properties of this state was rather well described by the use of the two degrees of freedom (shape vibration and two-quasiparticle excitation), the relevance of the two-quasiparticle excitations generally increasing with N along this chain of isotopes. Unfortunately, other 0^+ states and the two-neutron transfer intensities were not discussed in these papers. As a conclusion of this section, there are no microscopic model calculations applied to both Er isotopes ^{166}Er and ^{168}Er discussed here, which should attempt to explain the differences between them.

B. *spdf*-IBM-l calculations

In this section we present calculations with the interacting boson model (IBM) [66], in an effort to understand the structure of ^{166}Er and the subtle changes that appear when passing to its neighbor ^{168}Er. In this model correlated nucleon pairs are represented by bosonic degrees of freedom. The model has been extremely successful in reproducing, in a phenomenological way, the collective excitations at low energy, in many nuclear regions, including that of the rare-earth region.

The model is well suited for describing at the same time the electromagnetic and hadronic properties of the low-lying levels in even-even nuclei. Originally, the model used the s and d bosons (which carry angular momentum $L = 0$ and $L = 2$, respectively) as main ingredients. A recent investigation with different versions of this model (resulting from both mapping of a microscopic Hamiltonian on the IBM one, and from phenomenological approach) in the Sm, Gd, and Dy isotopes with $N = 84-94$ showed a reasonable description of the lowest few 0^+ and 2^+ states, including their population in the (p, t) and (t, p) transfer reactions, and the ability to signal the rapid structural changes at certain nucleon numbers [67].

However, bosons with different other angular momenta were found important to describe complex experimental data. Thus, Ref. [68] incorporated also the g boson ($L = 4$) in an attempt to better describe the population of the positive-parity states of ^{168}Er with the (t, p) reaction. A qualitative description of the $2n$-transfer strengths of Ref. [33] was obtained. More recently, in order to describe the large number of experimentally observed 0^+ states, and sometimes their transfer strengths in the (p, t) reaction, it proved very useful to introduce p and f bosons ($L = 1$ and $L = 3$, respectively) in addition to the s and d bosons [5,9,46,69–71]. The reason is that the model allows the presence of a number of double octupole/dipole states, meaning that additional $K^\pi = 0^+$ bands are obtained, which have a $N_{pf} = 2$ configuration. It follows that the IBM predicts an increased contribution of the octupole degree of freedom in the low-lying structure of various atomic nuclei. This is sometimes in contradiction with the prediction of other theoretical models, for example the quasiparticle phonon model (QPM), which indicates a moderate contribution of the octupole components in its wave functions while giving an increased weight to the pairing correlations [11]. The debate could be clarified by measurements of the appropriate observables related to the newly found states, especially the $E1$ transitions to the negative-parity octupole states.

We performed calculations within the *spdf* IBM-1 (no distinction between protons and neutrons is made) framework using the extended consistent Q formalism (ECQF) [72]. We employed the usual Hamiltonian:

$$\hat{H}_{spdf} = \epsilon_d \hat{n}_d + \epsilon_p \hat{n}_p + \epsilon_f \hat{n}_f + \kappa(\hat{Q}_{spdf} \cdot \hat{Q}_{spdf})^{(0)} + a_3[(\hat{d}^\dagger \tilde{d})^{(3)} \times (\hat{d}^\dagger \tilde{d})^{(3)}]^{(0)}, \quad (1)$$

where ϵ_d, ϵ_p, and ϵ_f are the boson energies and $\hat{n}_p$, $\hat{n}_d$, and $\hat{n}_f$ are the boson number operators. The quadrupole operator was taken as [73]:

$$\hat{Q}_{spdf} = \hat{Q}_{sd} + \hat{Q}_{pf} = (\hat{s}^\dagger \tilde{d} + \hat{d}^\dagger \hat{s})^{(2)} + \chi_{sd}^{(2)}(\hat{d}^\dagger \tilde{d})^{(2)} + \frac{3\sqrt{7}}{5}[(p^\dagger \tilde{f} + f^\dagger \tilde{p})]^{(2)} - \frac{9\sqrt{3}}{10}(p^\dagger \tilde{p})^{(2)} - \frac{3\sqrt{42}}{10}(f^\dagger \tilde{f})^{(2)}. \quad (2)$$

The quadrupole electromagnetic transition operator is:

$$\hat{T}(E2) = e_2 \hat{Q}_{spdf}, \quad (3)$$

where e_2 represents the boson effective charge.

As stated before, the good reproduction of the $E1$ transition strength is essential in evaluating the contribution of the octupole degree of freedom. Therefore, we also calculate $E1$ transitions in the IBM, using the following operator:

$$\hat{T}(E1) = e_1\big[\chi_{sp}^{(1)}(s^\dagger \tilde{p} + p^\dagger \tilde{s})^{(1)} + (p^\dagger \tilde{d} + d^\dagger \tilde{p})^{(1)} + \chi_{df}^{(1)}(d^\dagger \tilde{f} + f^\dagger \tilde{d})^{(1)}\big], \quad (4)$$

where e_1 is the effective charge for the $E1$ transitions and $\chi_{sp}^{(1)}$ and $\chi_{df}^{(1)}$ are two model parameters.

Since the Hamiltonian conserves separately the number of positive- and negative-parity bosons, one has to introduce an additional term to connect states with no (pf) content with those having $(pf)^2$ components. A very useful term was proven to be the dipole-dipole interaction term, which was used with success in previous calculations [9,69,70]:

$$\hat{H}_{\rm int} = \alpha \hat{D}_{spdf}^\dagger \cdot \hat{D}_{spdf} + \text{H.c.}, \quad (5)$$

TABLE IV. *spdf*-IBM parameters used in the present calculations, determined from a fitting procedure on the available experimental data.

Parameters		Nucleus		
		^{166}Er	^{168}Er	^{170}Er
Hamiltonian	ϵ_d (MeV)	0.4	0.37	0.37
	ϵ_p (MeV)	2.9	2.5	2.5
	ϵ_f (MeV)	1.6	2.5	2.5
	κ (MeV)	−0.03	−0.033	−0.033
	a_3 (MeV)	−0.13	−0.17	−0.13
	χ_{sd}	−0.3	−0.35	−0.25
	α (MeV)	0.0005	0.0005	0.0005
EM transition operators	e_2 (eb)	0.144	0.144	0.144
	e_1 (eb$^{1/2}$)	0.0095	0.0095	0.0095
	χ_{sp}	−0.86	−0.86	−0.86
	χ_{df}	0.59	0.59	0.59
Transfer operator	α_ν (mb/sr)	0.014		0.014
	α_p (mb/sr)	0		0.06
	α_f (mb/sr)	0.53		0.28

where

$$\hat{D}_{spdf} = -2\sqrt{2}[p^\dagger \tilde{d} + d^\dagger \tilde{p}]^{(1)} + \sqrt{5}[s^\dagger \tilde{p} + p^\dagger \tilde{s}]^{(1)} + \sqrt{7}[d^\dagger \tilde{f} + f^\dagger \tilde{d}]^{(1)}. \quad (6)$$

In previous calculations it was shown that there are two additional ingredients that make a successful calculation: the first is the inclusion of the octupole parameter in the Hamiltonian (last term), as shown in Eq. (1), while the second one is related to the use of an extended transfer operator, which includes terms proportional to the number of p and f bosons in addition to the leading-order term (third term) first used in Ref. [74]:

$$\hat{P}^{(0)}_\nu = (\alpha_p \hat{n}_p + \alpha_f \hat{n}_f)\hat{s} + \alpha_\nu \left(\Omega_\nu - N_\nu - \frac{N_\nu}{N}\hat{n}_d\right)^{\frac{1}{2}} \left(\frac{N_\nu + 1}{N+1}\right)^{\frac{1}{2}} \hat{s}, \quad (7)$$

where Ω_ν is the pair degeneracy of neutron shell, N_ν is the number of neutron pairs, N is the total number of bosons, and α_p, α_f, and α_ν are constant parameters.

The OCTUPOLE code [75] was used to diagonalize the Hamiltonian in Eqs. (1) and (5), to calculate the transition probabilities, and the transfer intensities. Up to three negative-parity bosons were allowed in the calculations and the parameters were fitted to the available experimental information. The structure of ^{166}Er and ^{168}Er is very similar at low excitation energy, although the present transfer experiment has revealed important discrepancies in the transfer strength pattern. Therefore, in order to reproduce the $2n$-transfer intensities in the calculations, one would need to substantially change the model parameters in Table IV, which is not in the spirit of the model. As a consequence, in the present calculations, emphasis was set on reproducing the properties of ^{166}Er, and less attention was given to the properties of the reaction transfers leading to ^{168}Er. In Table IV, we present the model parameters used for ^{166}Er, ^{168}Er, and ^{170}Er.

The results of the *spdf*-IBM calculations for ^{166}Er are displayed in Fig. 8. Since one of the main goals of the present

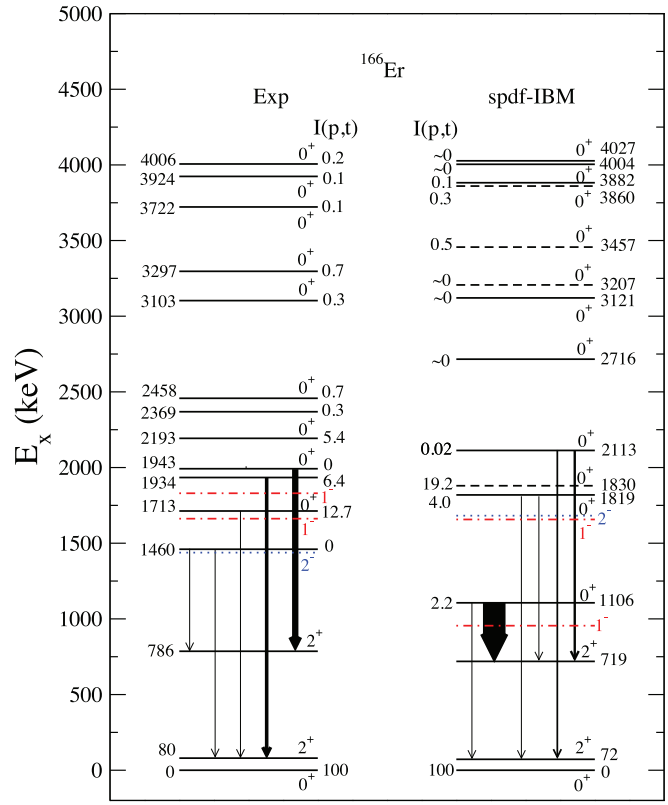

FIG. 8. Comparison between experimental and *spdf*-IBM calculated energy levels up to about 4 MeV in ^{166}Er. Besides the 0^+ states, which are all shown (with both firm and tentative assignment, see Table I) only the first two 2^+ states, first two 1^- states (red dash-dotted line), and the first 2^- state (blue dotted line), respectively, are also displayed. The transfer intensities in the (p, t) reaction for the 0^+ states and the $B(E2)$ electromagnetic transition probabilities (arrows) between the lowest levels are also indicated, the width of the arrows being proportional with the reduced strength. The calculated levels drawn with a dashed line have a two-octupole character.

experiment was the study of the monopole transfer strength, the figure displays mainly the 0^+ states, to which only the lowest 2^+, 1^-, and 2^- states are added. The number of 0^+ states up to about 4 MeV excitation in both experiment and calculations is the same. Also, a gap of about 600 keV around 2.5 MeV excitation, in the energy distribution of these states is reasonably well reproduced by the calculations. The transfer intensities in the (p, t) reaction are marked also on the figure, together with the corresponding electromagnetic $B(E2)$ transition probabilities for the lowest levels for which there was enough experimental information. The double-octupole states in the IBM calculations are represented with a dashed line. We notice that in the experiment there is no 0^+ state up to 2 MeV decaying to the negative parity levels, which would indicate a correlation with the octupole degrees of freedom. In contrast, several double-octupole states are predicted by the model, especially at higher excitation energy. It would be, therefore, very interesting to measure the decay transitions from the higher 0^+ levels in future experiments.

The experimental (p, t) transfer intensities are reasonably well reproduced by the calculations. The model predicts one

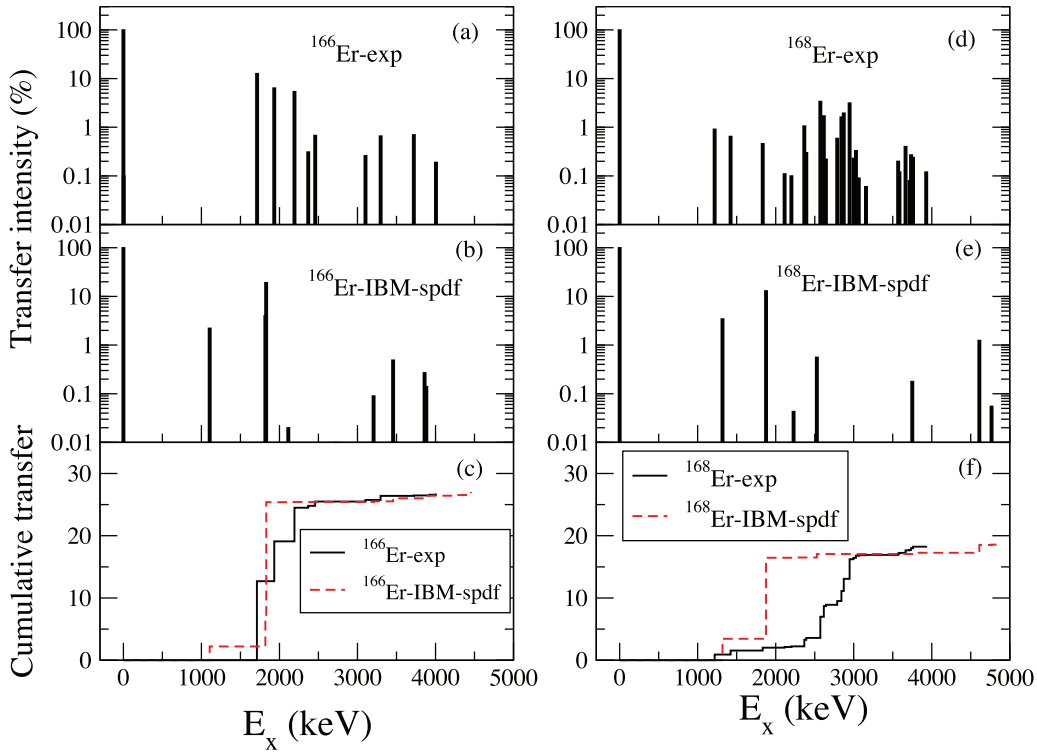

FIG. 9. Experimental and *spdf*-IBM calculated $2n$-transfer intensities in the (p, t) reaction to 0^+ states, both for individual levels and cumulated strength in ^{166}Er [(a)–(c)] and ^{168}Er [(d)–(f)].

state at 1830 keV, which carries most of the strength and two additional levels with lower intensity (at 1106 and 1819 keV), while in the experiment the intensity shows almost the same pattern with a strong state at 1713 keV and two weaker levels at 1934 and 2193 keV. At higher excitation energy, there is no level with transfer intensity larger than 1%, both in the experiment and in the calculations. The nature of the low-lying 0^+ states is rather well established following a series of experiments. The first excited state at 1460 keV in the experiment has a vanishing intensity and a small $B(E2)$ strength, and is proposed as having a dominant two-quasiparticle nature in Ref. [64]. If this picture is correct, this state is outside the IBM space and cannot be reproduced in our calculations. The next state at 1713 keV is interpreted as having a pairtype character [20], based on its strong transfer intensity and small $B(E2)$ value. In the IBM, the model produces a state at 1830 keV with a strong transfer intensity and small $B(E2)$ values towards the first and second 2^+ levels. It has a double-octupole character and strongly decays to the first excited 1^- state. The β-vibration state was established experimentally at 1934 keV based on its strong transition probability towards the 2_1^+ level [20]. The strongest transition produced by the IBM calculations towards the 2_1^+ state belongs to the level at 2113 keV, which also has a small transfer intensity characteristic of a β-vibration state. Finally, the level at 1943 keV was found to have a double-γ phonon structure based on its strong decay towards the 2_2^+ level [21]. In IBM, such a state is located at 1106 keV. For the higher-lying states, it would be difficult to try to find a one-to-one correspondence with the experimental levels. Such identification might be facilitated by the measurement of their γ decay pattern.

The quality of the (p, t) reaction transfer intensity calculations, both for ^{166}Er and ^{168}Er, can be inferred from Fig. 9. For ^{166}Er (left-side panels) there is a reasonable agreement between the experiment and the calculations. The most intensely populated levels lie around 2 MeV excitation in both cases, and above that the intensity is fragmented over many states and reaches about 27% around 4 MeV. By contrast, the calculations do not describe the main feature of the data in ^{168}Er, that is, the bunch of relatively strongly populated levels around 2.7 MeV. This result is due to the fact that we used similar Hamiltonian parameters for both nuclei. As stated above a large change in the parameters used for the two nuclei would not be advisable, although it was shown in Ref. [76] that a smooth evolution of the parameters in the Er isotopic chain can be achieved in the IBM only by considering the 0_3^+ level in ^{168}Er as the first collective excitation of this nucleus. This is another indication, although indirect, that the structure of ^{168}Er is different as compared to the other neighboring nuclei.

Figure 10 shows that the calculations can reasonably describe, with the same parameters as discussed above, the main features experimentally determined for the ^{166}Er$(t, p)^{168}$Er reaction. The experiment [33] found relatively large intensities for the first three excited 0^+ states (1217, 1422, and 1833 keV, respectively) in ^{168}Er; the calculations predict similar strengths and a comparable cumulated strength in the first four excited 0^+ states.

We finally discuss another issue, the experimental and calculated $E1$ transition rates. A good simultaneous description of both transfer strengths and transition probabilities would give more confidence in the structure image proposed by the

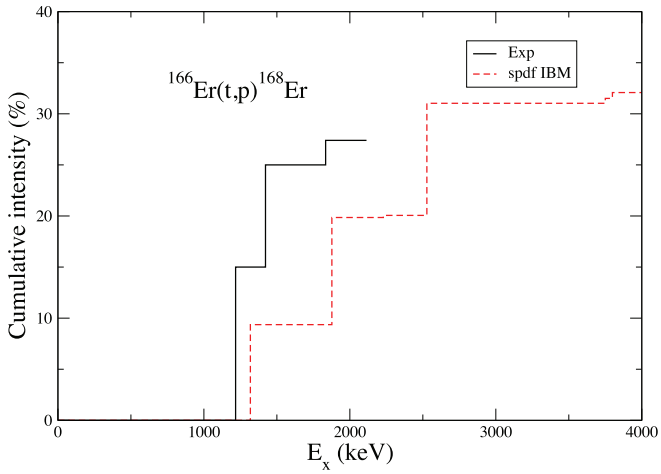

FIG. 10. Experimental and *spdf*-IBM calculations of $2n$-transfer strengths for (t, p) reaction leading to 0^+ excited states of ^{168}Er. The transfer intensities are given in percent, relative to the gs → gs transition.

IBM. Although ^{166}Er is not located in a region where octupole degrees of freedom play a major role, several negative-parity bands have been identified in this nucleus, and therefore, should be tested against theoretical predictions. We have presented in Fig. 8 the first few negative-parity states produced by the model, namely the first two 1^- states and the first 2^- level. We note that in the case of ^{166}Er, the order of the octupole bands is given as $K = 2^-, 0^-, 3^-, 1^-$ in the experimental data [16]. In the IBM, based on the Hamiltonian in Eq. (1), the first excited negative-parity states are produced with $K^\pi = 0^-$, 1^-, 2^-, 3^-. The ordering of these bands can be changed by introducing in the Hamiltonian a term proportional with $(d^\dagger \tilde{f})^{(3)} \cdot (f^\dagger \tilde{d})^{(3)}$ [77]. Since the goal of the present study was not a detailed reproduction of the negative-parity states, we have chosen not to introduce any additional parameters in the Hamiltonian and keep the parameters to a minimum. However, since the octupole degrees of freedom play an important role in the calculations of 0^+ states, we concentrate mainly on reproducing the octupole strength in ^{166}Er for the first negative-parity levels for which a detailed knowledge about their decay pattern is known. Therefore, we present in Table V the results of this comparison in the case of the $B(E1)$ ratios [defined as $R(E1) = \frac{B(E1;J_i \to J_{f1})}{B(E1;J_i \to J_{f2})}$] for the levels belonging to $K^\pi = 0^-$ and $K^\pi = 2^-$ structures. In IBM, the $E1$ transitions are calculated using Eq. (4) and the parameters from Table V. The results show a very good agreement between experiment and IBM, indicating that the octupole strength is not overestimated in the present calculations, although details of the wave functions have not been considered.

V. CONCLUSIONS

We have presented a detailed investigation of excited states of the deformed nucleus ^{166}Er, with a high-energy resolution (p, t) reaction experiment. Up to about 4 MeV excitation, a number of 140 excited states have been observed, among which 11 excited 0^+ states, 39 2^+ states, and about 40 states with other spin values have been assigned on the basis of DWBA analysis of the angular distributions. These results allowed a detailed comparison with the ^{168}Er neighbor nucleus, previously studied in a similar experiment. Although at low excitation energies the two nuclei have almost identical structure, there are important differences between them in the excitation patterns of the 0^+ and 2^+ states in the (p, t) reaction.

Although it is clear, from various experimental studies and theoretical calculations, that these states may not all be collective, we performed calculations with the *spdf*-IBM model. These calculations reproduce, at least qualitatively, for ^{166}Er, general features such as the number of excited 0^+ state, their distribution of the $2n$-transfer strengths in both the (p, t) and (t, p) reactions, $E2$ and $E1$ electromagnetic decays. This may be taken as a proof of the possibility that octupole correlations may play a certain role in the low-energy regime of this nucleus.

On the other hand, for the ^{168}Er nucleus, similar calculations with Hamiltonian parameters close to those of ^{166}Er, do not reproduce the experimental distribution of the $2n$-transfer strengths, a situation similar to that of QPM and PSM calculations of a previous study [4]. The evolution of different spectroscopic properties, such as excitation energies of low-lying states indicates an important structure change taking place at the $N = 98$ deformed shell closure. Thus, further calculations of all these properties with models, which should take into account both collective and noncollective degrees of freedom remain of considerable interest.

TABLE V. Experimental and calculated $B(E1)$ ratios [defined as $R(E1) = \frac{B(E1;J_i \to J_{f1})}{B(E1;J_i \to J_{f2})}$] in ^{166}Er. The parameters of the $E1$ operator in Eq. (4) are given in Table IV.

K^π	E_i (keV)	J_i	J_{f1}	J_{f2}	Expt.	IBM
0^-	1662	1^-	2_1^+	0_1^+	1.78(20)	2.28
	1721	3^-	4_1^+	2_1^+	1.12(22)	1.86
2^-	1458	2^-	3_γ^+	2_γ^+	0.49(2)	0.72
		2^-	2_1^+	2_γ^+	0.00014(7)	0.00002
	1513	3^-	4_γ^+	2_1^+	11.4(20)	18.8
		3^-	3_γ^+	2_1^+	9.0(15)	7.0
		3^-	2_γ^+	2_1^+	7.0(12)	5.2
		3^-	4_1^+	2_1^+	0.77(13)	1.38
	1596	4^-	5_γ^+	3_γ^+	1.9(1)	3.2
		4^-	4_γ^+	3_γ^+	0.57(4)	0.55
		4^-	4_1^+	4_1^+	0.0030(4)	0.001
	1692	5^-	6_γ^+	4_1^+	2.0(1)	2.2
		5^-	5_γ^+	4_1^+	0.6(2)	0.06
		5^-	4_γ^+	4_1^+	2.0(2)	0.47
		5^-	6_1^+	2_1^+	0.79(1)	1.26

ACKNOWLEDGMENTS

We acknowledge partial support for this work within the UEFSICDI-Romania project PN-II-ID-PCE-2011-3-0140, and the DFG Grant 436 RUM 17/1/07.

[1] S. R. Lesher, A. Aprahamian, L. Trache, A. Oros-Peusquens, S. Deyliz, A. Gollwitzer, R. Hertenberger, B. D. Valnion, and G. Graw, Phys. Rev. C **66**, 051305(R) (2002).

[2] D. A. Meyer, V. Wood, R. F. Casten, C. R. Fitzpatrick, G. Graw, D. Bucurescu, J. Jolie, P. von Brentano, R. Hertenberger, H.-F. Wirth, N. Braun, T. Faestermann, S. Heinze, J. L. Jerke, R. Krücken, M. Mahgoub, O. Möller, D. Mücher, and C. Scholl, Phys. Rev. C **74**, 044309 (2006).

[3] D. A. Meyer *et al.*, Phys. Lett. B **638**, 44 (2006).

[4] D. Bucurescu, G. Graw, R. Hertenberger, H.-F. Wirth, N. Lo Iudice, A. V. Sushkov, N. Yu. Shirikova, Y. Sun, T. Faestermann, R. Krücken, M. Mahgoub, J. Jolie, P. von Brentano, N. Braun, S. Heinze, O. Möller, D. Mücher, C. Scholl, R. F. Casten, and D. A. Meyer, Phys. Rev. C **73**, 064309 (2006).

[5] L. Bettermann, S. Heinze, J. Jolie, D. Mücher, O. Möller, C. Scholl, R. F. Casten, D. Meyer, G. Graw, R. Hertenberger, H.-F. Wirth, and D. Bucurescu, Phys. Rev. C **80**, 044333 (2009).

[6] G. Ilie, R. F. Casten, P. von Brentano, D. Bucurescu, T. Faestermann, G. Graw, S. Heinze, R. Hertenberger, J. Jolie, R. Krücken, D. A. Meyer, D. Mücher, C. Scholl, V. Werner, R. Winkler, and H.-F. Wirth, Phys. Rev. C **82**, 024303 (2010).

[7] C. Bernards, R. F. Casten, V. Werner, P. von Brentano, D. Bucurescu, G. Graw, S. Heinze, R. Hertenberger, J. Jolie, S. Lalkovski, D. A. Meyer, D. Mücher, P. Pejovic, C. Scholl, and H.-F. Wirth, Phys. Rev. C **87**, 024318 (2013).

[8] C. Bernards, R. F. Casten, V. Werner, P. von Brentano, D. Bucurescu, G. Graw, S. Heinze, R. Hertenberger, J. Jolie, S. Lalkovski, D. A. Meyer, D. Mücher, P. Pejovic, C. Scholl, and H.-F. Wirth, Phys. Rev. C **87**, 064321 (2013).

[9] N. V. Zamfir, J.-Y. Zhang, and R. F. Casten, Phys. Rev. C **66**, 057303 (2002).

[10] N. Lo Iudice, A. V. Sushkov, and N. Y. Shirikova, Phys. Rev. C **70**, 064316 (2004).

[11] N. Lo Iudice, A. V. Sushkov, and N. Y. Shirikova, Phys. Rev. C **72**, 034303 (2005).

[12] N. Lo Iudice and A. V. Sushkov, Phys. Rev. C **78**, 054304 (2008).

[13] Y. Sun, A. Aprahamian, J.-Y. Zhang, and C.-T. Lee, Phys. Rev. C **68**, 061301(R) (2003).

[14] M. Gerçeklioglu, Eur. Phys. J. A **25**, 185 (2005)

[15] D. Bonatsos, E. A. McCutchan, R. F. Casten, R. J. Casperson, V. Werner, and E. Williams, Phys. Rev. C **80**, 034311 (2009).

[16] C. M. Baglin, Nucl. Data Sheets **109**, 1103 (2008); retrieved from the ENSDF database, http://www.nndc.bnl.gov/ensdf/.

[17] R. L. Gill, C. Barton, R. F. Casten, and N. V. Zamfir, Phys. Rev. C **51**, 2801 (1995).

[18] C. Ardisson, V. Barci, J. Dalmasso, A. Hachem, and G. Ardisson, Il Nuovo Cim. A **105**, 215 (1992).

[19] W. D. Kulp, J. M. Allmond, P. Hatcher, J. L. Wood, J. Loats, P. Schmelzenbach, C. J. Stapels, K. S. Krane, R.-M. Larimer, and E. B. Norman, Phys. Rev. C **73**, 014308 (2006).

[20] P. E. Garrett, M. Kadi, C. A. McGrath, V. Sorokin, Min Li, Minfang Yeh, and S. W. Yates, Phys. Lett. B **400**, 250 (1997).

[21] P. E. Garrett, M. Kadi, M. Li, C. A. McGrath, V. Sorokin, M. Yeh, and S. W. Yates, Phys. Rev. Lett. **78**, 4545 (1997).

[22] L. I. Govor, A. M. Demidov, and S. A. Berendakov, Phys. At. Nucl. **78**, 171 (2015).

[23] XUNDL, Experimental Unevaluated Nuclear Data List, maintained by the National Nuclear Data Center, Brookhaven National Laboratory, https://www.nndc.bnl.gov/ensdf/ensdf/xundl.jsp.

[24] T. Ichihara, H. Sakaguchi, M. Nakamura, M. Yosoi, M. Ieiri, Y. Takeuchi, H. Togawa, T. Tsutsumi, and S. Kobayashi, Phys. Rev. C **36**, 1754 (1987).

[25] P. O. Tjom and B. Elbek, Nucl. Phys. A **107**, 385 (1968).

[26] C. Fahlander *et al.*, Acta Phys. Hung. N. S. **7**, 109 (1998); C. Fahlander, A. Axelsson, M. Heinebrodt,T. Härtlein, and D. Schwalm, Phys. Lett. B **388**, 475 (1996).

[27] H. Li, P. V. Magnus, M. S. Smith, P. D. Parker, J. A. Cizewski, C. S. Lee, D. Barker, C. Wesselborg, and A. E. Champagne, Phys. Rev. C **47**, 1943 (1993).

[28] D. G. Burke, D. E. Nelson, and C. W. Reich, Nucl. Phys. A **124**, 683 (1969).

[29] J. D. Panar and D. G. Burke, Can. J. Phys. **57**, 1999 (1979).

[30] H. Maser, S. Lindenstruth, I. Bauske, O. Beck, P. von Brentano, T. Eckert, H. Friedrichs, R. D. Heil, R.-D. Herzberg, A. Jung, U. Kneissl, J. Margraf, N. Pietralla, H. H. Pitz, C. Wesselborg, and A. Zilges, Phys. Rev. C **53**, 2749 (1996).

[31] C. A. Fields, K. H. Hicks, and R. J. Peterson, Nucl. Phys. A **440**, 301 (1985).

[32] D. G. Burke and P. E. Garrett, Nucl. Phys. A **550**, 21 (1992).

[33] D. G. Burke, W. F. Davidson, J. A. Cizewski, R. E. Brown, E. R. Flynn, and J. W. Suniwer, Can. J. Phys. **63**, 1309 (1985).

[34] P. E. Garrett, C. Burbadge, D. Kisliuk, G. C. Ball, V. Bildstein, A. Diaz Varela, M. R. Dunlop, R. Dunlop, T. Faestermann, R. Hertenberger, D. S. Jamielson, K. G. Leach, J. Loranger, A. D. MacLean, A. J. Radich, E. T. Rand, B. Rebeiro, C. E. Svensson, S. Triambak, and H.-F. Wirth, in *Proceedings of the 26th International Nuclear Physics Conference 2016, Adelaide, Australia* (SISSA, 2017).

[35] C. Burbadge, P. E. Garrett, G. C. Ball, V. Bildstein, A. Diaz Varela, M. R. Dunlop, R. Dunlop, T. Faestermann, R. Hertenberger, D. S. Jamielson, K. G. Leach, J. Loranger, A. D. MacLean, A. J. Radich, E. T. Rand, C. E. Svensson, S. Triambak, and H.-F. Wirth, EPJ Web Conf. **178**, 02025 (2018).

[36] J. V. Maher, J. J. Kolata, and R. W. Miller, Phys. Rev. C **6**, 358 (1972).

[37] R. F. Casten and P. von Brentano, Phys. Rev. C **51**, 3528 (1995).

[38] D. G. Burke and P. C. Sood, Phys. Rev. C **51**, 3525 (1995).

[39] M. Löffler, H. J. Scheerer, and H. Vonach, Nucl. Instrum. Methods **111**, 1 (1973).

[40] H.-F. Wirth, H. Angerer, T. von Egidy, Y. Eisermann, G. Graw, and R. Hertenberger, Beschleunigerlaboratorium München Annual Report No. 3.6, 2000, p. 71.

[41] H.-F. Wirth, Ph.D. thesis, Technische Universität München, München, 2001, http://mediatum.ub.tum.de?id=602907.

[42] E. Browne, Nucl. Data Sheets **88**, 29 (1999); and ENSDF database at http://www.nndc.bnl.gov.

[43] P. D. Kunz, Computer code CHUCK3, University of Colorado.

[44] C. M. Perey and F. G. Perey, At. Data Nucl. Data Tables **17**, 1 (1976).

[45] J. Adam, A. Budziak, W. Wagner, V. Zvolska, I. Zvolski, B. Kracik, and M. Fisher, Bull. Acad. Sci. USSR, Phys. Ser. **53**, 875 (1989).

[46] A. I. Levon, G. Graw, Y. Eisermann, R. Hertenberger, J. Jolie, N. Y. Shirikova, A. E. Stuchbery, A. V. Sushkov, P. G. Thirolf, H.-F. Wirth, and N. V. Zamfir, Phys. Rev. C **79**, 014318 (2009).

[47] D. R. Bes, Nucl. Phys. **49**, 544 (1963).

[48] D. R. Bes and R. A. Broglia, Nucl. Phys. **80**, 289 (1966).

[49] A. A. Kuliev and N. I. Pyatov, Nucl. Phys. A **106**, 689 (1968).
[50] R. Broglia, O. Hansen, and C. Riedel, Adv. Nucl. Phys. **6**, 287 (1973).
[51] P. Garrett, J. Phys. G: Nucl. Part. Phys. **27**, R1 (2001).
[52] M. A. M. Shahabudin and D. G. Burke, Can. J. Phys. **58**, 832 (1980).
[53] D. G. Burke, G. Løvhøiden and T. F. Thorsteinsen, Nucl. Phys. A **483**, 221 (1988).
[54] R. M. Clark, R. F. Casten, L. Bettermann, and R. Winkler, Phys. Rev. C **80**, 011303(R) (2009).
[55] T. Engeland and J. S. Vaagen, Phys. Scr. **34**, 703 (1986).
[56] M. A. Asgar, T. Roy, G. Mukherjee, A. Dhal, S. Bhattacharya, S. Bhattacharyya, C. Bhattacharya, S. Bhattacharya, A. Chaudhuri, K. Banerjee, S. Kundu, S. Manna, R. Pandey, J. K. Meena, R. Palit, S. Biswas, S. Saha, J. Sethi, P. Singh, and D. Choudhury, Phys. Rev. C **95**, 031304(R) (2017).
[57] V. G. Soloviev, A. V. Sushkov, and N. Yu. Shirikova, Phys. Rev. C **51**, 551 (1995).
[58] K. Hara and Y. Sun, Int. J. Mod. Phys. E **04**, 637 (1995).
[59] M. Gerceklioglu, Eur. Phys. J. A **48**, 12141 (2012).
[60] J.-P. Delaroche, M. Girod, J. Libert, H. Goutte, S. Hilaire, S. Peru, N. Pillet, and G. F. Bertsch, Phys. Rev. C **81**, 014303 (2010).
[61] J. Terasaki and J. Engel, Phys. Rev. C **84**, 014332 (2011).
[62] N. Hinohara, M. Kortelainen, and W. Nazarewicz, Phys. Rev. C **87**, 064309 (2013).
[63] P. Ring and P. Schuck, *The Nuclear Many Body Problem* (Springer, New York, 1980).
[64] F.-Q. Chen and J. L. Egido, Phys. Rev. C **93**, 064313 (2016).
[65] F.-Q. Chen and J. L. Egido, Phys. Rev. C **95**, 024307 (2017).
[66] F. Iachello and A. Arima, *The Interacting Boson Model* (Cambridge University Press, Cambridge, 1987).
[67] K. Nomura and Y. Zhang, Phys. Rev. C **99**, 024324 (2019).
[68] Y. Akiyama, K. Heyde, A. Arima, and N. Yoshinaga, Phys. Lett. B **173**, 1 (1986).
[69] A. I. Levon, G. Graw, R. Hertenberger, S. Pascu, P. G. Thirolf, H.-F. Wirth, and P. Alexa, Phys. Rev. C **88**, 014310 (2013).
[70] A. I. Levon, P. Alexa, G. Graw, R. Hertenberger, S. Pascu, P. G. Thirolf, and H.-F. Wirth, Phys. Rev. C **92**, 064319 (2015).
[71] M. Spieker, S. Pascu, D. Bucurescu, T. M. Shneidman, T. Faestermann, R. Hertenberger, H.-F. Wirth, N.-V. Zamfir, and A. Zilges, Phys. Rev. C **97**, 064319 (2018).
[72] R. F. Casten and D. D. Warner, Rev. Mod. Phys. **60**, 389 (1988).
[73] D. Kusnezov, J. Phys. A **23**, 5673 (1990).
[74] O. Scholten, F. Iachello, and A. Arima, Ann. Phys. (NY) **115**, 325 (1978).
[75] D. Kusnezov, computer code OCTUPOLE.
[76] E. A. McCutchan, N. V. Zamfir, and R. F. Casten, Phys. Rev. C **69**, 064306 (2004).
[77] P. D. Cottle and N. V. Zamfir, Phys. Rev. C **54**, 176 (1996).